IIETA International Information and Engineering Technology Association
Advancing the World of Information and Engineering

Traitement du Signal
Vol. 40, No. 5, October, 2023, pp. 1843-1856
Journal homepage: http://iieta.org/journals/ts

Predicting Flow-Induced Noise Based on an Improved Four-Dimensional Acoustic Analogy Model and Multi-Domain Feature Analysis

Wensi Zheng[1], Qiuhong Liu[1], Jinsheng Cai[1], Fang Wang[2*]

[1] School of Aeronautics, Northwestern Polytechnical University, Xi'an 710072, China
[2] School of Civil Engineering, North Minzu University, Yinchuan 750021, China

Corresponding Author Email: wangf@nmu.edu.cn

https://doi.org/10.18280/ts.400506

Received: 19 April 2023
Revised: 6 July 2023
Accepted: 2 August 2023
Available online: 30 October 2023

Keywords:
electromagnetic analogy, acoustic pressure signal, acoustic velocity signal, multi-domain feature, four-dimensional acoustic analogy, Navier-Stokes equation, load source term

ABSTRACT

Flow-induced noise issues are widely present in practical engineering fields. Accurate prediction of noise signals is fundamental to studying the mechanism of noise generation and seeking effective noise suppression methods. Complete acoustic field information often includes both acoustic pressure and velocity vectors. However, the classic acoustic analogy theory can only consider the feature distribution of acoustic pressure. This study starts from the dimensionless Navier-Stokes equations followed by fluid motion and, with the concept of electromagnetic analogy, introduces a vector form of the fluctuation equation that includes density perturbations and velocities in three directions. By choosing the permeable integral surface surrounding the object as the sound source surface, this study further analyzes the composition of the volume source term and extract the complete load source term, proposing the time-domain integral analytical formula T4DC and the frequency-domain integral formula F4DC. Numerical predictions for stationary dipoles and rotating monopoles are carried out in the time domain, frequency domain, and spatial domain. The numerical results show that the time-domain and frequency-domain noise obtained by this method can be consistent with the analytical solution, while the method of Dunn has a significant difference from the analytical solution, especially for dipole noise distribution. Compared with the accurate solution, the acoustic velocity amplitude error obtained by Dunn's method reached more than 35% at m=1 frequency, fully demonstrating that our method can accurately predict far-field acoustic pressure and velocity vectors.

1. INTRODUCTION

Aeroacoustic noise, also known as flow-induced noise, is essential for studying the mechanisms of noise generation and finding effective noise suppression methods. With the continuous enhancement of computational capabilities, using numerical methods to predict aeroacoustic noise has become a popular approach. Classical acoustic analogy methods have established the response relationship between the sound field and various types of sound sources and have become the most widely used numerical prediction method for aeroacoustic noise. The core idea is to first calculate the aeroacoustic source information within a finite domain using high-precision Computational Fluid Dynamics (CFD) methods, and then use the acoustic analogy integral equation, such as the FW-H equation [1], to extrapolate the sound wave propagation from the near field to the far field. Generally, the FW-H equation uses a closed permeable surface [2] as the integration surface, and the complete solution consists of surface and volume integrals. When the main aeroacoustic source is enclosed within the permeable surface, the contribution of the volume integral to the sound field can be neglected [3], and only the thickness source and load source information on the permeable surface are used to extrapolate the external sound field, such as the semi-analytical formula F1 and analytical formula F1A proposed by Farassat [4], which can accurately obtain the characteristic distribution of sound pressure.

In fact, a complete sound field consists of sound pressure (scalar) and three components of acoustic velocity (vector), meaning the sound field is four-dimensional. This presents new requirements for the acoustic computation model: it should describe the propagation state of sound waves and clearly explain the energy transport of sound waves. Regrettably, the aforementioned classical models [1-4] only consider the propagation state of sound pressure. The study of sound wave energy transport often employs the sound intensity vector, which is defined as a function of sound pressure and acoustic velocity. Visualization of the sound intensity field can display the propagation path of noise energy in detail [5]. Non-compact structures on the noise propagation path can cause sound scattering, changing the size, waveform, and directionality of the sound field. The concept of sound scattering has many variations in practical applications [6, 7], but all require predicting the acoustic velocity at the scattering boundary as the boundary condition. Using sound intensity visualization technology, Lee et al. [8] revealed the impact of scattering surfaces on sound energy redistribution, and Crocker and Jacobsen [9] mainly discussed the theoretical and practical application of sound-intensity measurement, especially in engineering problems. It can be seen from the above that the classical acoustic analogy method only focuses on the prediction of sound pressure and does not stipulate the extrapolation of the acoustic velocity vector, making it incomplete [10].

It can be observed that the combination of classical acoustic analogy methods can accurately obtain the distribution of sound pressure. However, the precise prediction of the sound field is influenced by both sound pressure and the acoustic velocity vector. According to the linear Euler equation, the sound pressure gradient can indirectly represent the acoustic velocity. For a stationary sound propagation medium, Farassat and Brentner [11] proposed a semi-analytical formula to calculate the sound pressure gradient. Lee et al. [12] derived the semi-analytical formulas G1 and G1A for sound pressure gradient calculation and evaluated the sound scattering of rotor noise combined with the equivalent source method [13]. However, for large-scale sound scattering problems, such as the sound scattering of aircraft fuselages or wings, the integration efficiency of sound pressure gradients is low, making it difficult to obtain the acoustic velocity vector precisely and quickly. Therefore, improving the efficiency of acoustic vector field prediction is essential for solving practical aeroacoustic problems, and there is a need to develop clearer, more efficient, and vectorizable acoustic prediction formulas. For stationary homogeneous media, Ghorbaniasl et al. [14] proposed the time-domain formulas V1 and V1A for acoustic velocity calculation based on the integral solution of the FW-H equation. Mao et al. [15] extended the formula V1A to the frequency domain, resulting in formulas FV1A and FV2A, which calculated the acoustic velocity induced by a constant rotational speed harmonic point source, and revealed three modes of rotating point source radiated noise using the sound energy streamline diagram [16], namely the helical mode, R-A mode, and acoustic black hole mode. Mao et al. [17] further proposed a frequency domain equivalent source method to predict the sound scattering of rotating thickness sources and load sources. Additionally, Mao et al. [18] introduced a vector wave equation with acoustic velocity as the variable, proposing another method to derive formulas V1 and V1A. As Lee and Brentner [19] pointed out, the acoustic velocity formulas V1 and V1A can actually be directly derived from the sound pressure gradient formulas G1 and G1A. He et al. [20] pointed out that formulas V1 and V1A are not suitable for acoustic near-fields and developed more efficient acoustic velocity integration formulas V2 and V2A. The above research methods focus on accurately obtaining the acoustic velocity vector, expanding and generalizing the classical acoustic analogy model, and examining the physical features of the acoustic velocity fields of stationary point sources and moving point sources. However, the above methods did not comprehensively consider the distribution of sound field characteristics and the laws of sound energy transport under the influence of acoustic scalars and vectors.

How to obtain accurate computational formulas for sound pressure and acoustic velocity vector fields from the physical perspective of flow-induced noise is a problem that needs to be addressed. In fact, fluid mass and momentum conservation equations are similar in form to Maxwell's equations in vacuum electrodynamics. Scholars have proposed that some combinations of flow field variables and their derivatives can be defined as "fluid electric fields" and "fluid magnetic fields," thereby converting fluid dynamics equations into "fluid Maxwell's equations" [21, 22]. Dunn [10], using the concept of electromagnetic analogy, reorganized the mass and conservation equations of fluid motion, establishing a four-dimensional acoustic analogy formulation that includes both sound pressure scalars and acoustic velocity vectors (three components). The four-dimensional acoustic analogy formula is easy to implement and can predict the characteristic distributions of both acoustic pressure and velocity. However, Dunn's method [10] is only reliable when the object surface is chosen as the integration boundary. When using a permeable surface as the integration boundary, the surface source terms related to acoustic velocity in Dunn's four-dimensional acoustic analogy integration formula are not fully extracted, leading to inaccurate prediction results for acoustic velocity. However, complex structural acoustic calculation problems are widespread in practical engineering issues. Surface integration of complex structures often presents numerical singularity and high numerical computational complexity. Permeable integration surfaces that enclose complex structure surfaces can avoid these problems.

Considering the significant advantages of four-dimensional sound field calculation and the needs of practical engineering problems, this study extensively carries out research on the four-dimensional acoustic analogy theory and conducts numerical prediction research on vector noise in multi-domain space for stationary dipoles and moving monopoles. The second part proposes a modified four-dimensional FW-H equation, with pressure and three-directional acoustic velocities as the four-dimensional vector, combined with the basic solution of the Green's function to obtain the time/frequency domain calculation formula of four-dimensional acoustics, enabling prediction research of far-field four-dimensional acoustic vectors. The third part demonstrates using time-domain and frequency-domain integration formulas for sound propagation prediction, examining the sound field development of stationary dipoles and rotating monopoles, comparing the results with theoretical solutions, and analyzing the relationship between sound propagation mode and rotational speed. The fourth part discusses the influence of aeroacoustic scattering on four-dimensional acoustic fields. The fifth part gives a summary and discussion of the research results.

2. FORMULATIONS

2.1 Four-dimensional FW-H equation

Considering the propagation of sound waves in a homogeneous stationary medium, starting from the dimensionless continuity equation and momentum equation [10], there are:

$$\frac{\partial \rho'}{\partial t}+\frac{\partial\left(\rho u_j\right)}{\partial x_j}=0 \tag{1}$$

$$\frac{\partial\left(\rho u_i\right)}{\partial t}+\frac{\partial \rho'}{\partial x_i}=-\frac{\partial T_{ij}}{\partial x_j} \tag{2}$$

where, the Lighthill stress tensor is:

$$T_{ij}=\rho u_i u_j+\left(p'-\rho'\right)\delta_{ij}-\sigma_{ij} \tag{3}$$

Eq. (1) describes the mass conservation relationship followed during the fluid motion process. Eqs. (2)-(3) express the momentum conservation relationship in the fluid motion process. The derivation proof of above equations can be found in Appendix 1. In Eqs. (1) to (3), all physical quantities are

described dimensionlessly. For their dimensionless descriptions and definitions, please refer to Appendix 1 as well. p and r represent transient pressure and density, respectively. p_0 represents pressure under equilibrium. Corresponding to the Cartesian coordinate system, u_i represents the fluid velocity along the i direction (i=1,2,3). δ_{ij} and σ_{ij} represent the Kronecker delta tensor and the viscous stress tensor, respectively. Pressure fluctuation and velocity fluctuation are defined as:

$$p' = p - p_0, \quad \rho' = \rho - 1 \tag{4}$$

Through defining first-order four-dimensional tensors:

$$\begin{aligned} \phi^\alpha &= \begin{pmatrix} \phi^0 \\ \phi^1 \\ \phi^2 \\ \phi^3 \end{pmatrix} = \begin{pmatrix} \rho' \\ \rho u_1 \\ \rho u_2 \\ \rho u_3 \end{pmatrix} = \begin{pmatrix} \rho' \\ --- \\ \rho u_i \end{pmatrix}, \\ X^\alpha &= \begin{pmatrix} X^0 \\ X^1 \\ X^2 \\ X^3 \end{pmatrix} = \begin{pmatrix} t \\ x_1 \\ x_2 \\ x_3 \end{pmatrix} = \begin{pmatrix} t \\ --- \\ x_i \end{pmatrix} \end{aligned} \tag{5}$$

The four-dimensional differential operator:

$$\frac{\partial}{\partial X^\alpha} = \begin{pmatrix} \dfrac{\partial}{\partial t} \\ ---- \\ \dfrac{\partial}{\partial x_i} \end{pmatrix}, \quad \alpha = 0,\ 1,\ 2,\ 3 \tag{6}$$

The "fluid electric field" vector $\boldsymbol{E}$ and "fluid magnetic field" vector $\boldsymbol{B}$:

$$\begin{aligned} \mathbf{E} &= -\frac{\partial(\rho \mathbf{u})}{\partial t} - \nabla \rho' = \frac{\partial \mathbf{e}^\gamma}{\partial X^\gamma}, \\ \mathbf{B} &= \nabla \times (\rho \mathbf{u}) = \frac{\partial \mathbf{b}^\gamma}{\partial X^\gamma} \end{aligned} \tag{7}$$

Here, considering that the expressions of fluid mass and momentum conservation Eqs. (1)-(3) are similar to the Maxwell equations of vacuum electromagnetism, we borrow the concepts of electric and magnetic fields to define fluid physical variables. Specifics can be found in references [10, 11].

Dunn [10] reorganized Eqs. (1) and (2) into:

$$\Box^2 \phi^\beta = \frac{\partial^2 V^{\alpha\beta\gamma}}{\partial X^\alpha \partial X^\gamma} \tag{8}$$

where, the left side of the equation $\Box^2$ represents the dimensionless wave operator, and the right side $V^{\alpha\beta\gamma}$ is defined as:

$$V^{\alpha\beta\gamma} = Z^{\alpha\beta}\left(\mathbf{e}^\gamma, \mathbf{b}^\gamma\right) = \begin{pmatrix} 0 & -e_1^\gamma & -e_2^\gamma & -e_3^\gamma \\ e_1^\gamma & 0 & -b_3^\gamma & b_2^\gamma \\ e_2^\gamma & b_3^\gamma & 0 & -b_1^\gamma \\ e_3^\gamma & -b_2^\gamma & b_1^\gamma & 0 \end{pmatrix} \tag{9}$$

Eq. (8) is similar to the physical equation of sound propagation in form, and the difference is that it can describe the propagation rules of four-dimensional vector signals in physical space, and the $V^{\alpha\beta\gamma}$ on the right side represents the sound source term.

By introducing a closed permeable surface $f(\boldsymbol{x}, t) = 0$ with a motion speed of v, defining the internal and external regions of the permeable surface as $f(\boldsymbol{x}, t) < 0$ and $f(\boldsymbol{x}, t) > 0$, and ensuring that the unit outward normal vector of the permeable surface satisfies $\boldsymbol{n} = \nabla f$, then there is:

$$\frac{\partial f}{\partial X^\alpha} = N_\alpha = \begin{pmatrix} -v_j n_j \\ ----- \\ n_i \end{pmatrix} \tag{10}$$

Based on Eq. (10), Eq. (8) can be further written as:

$$\Box^2\left[\phi^\beta H(f)\right] = \underbrace{\frac{\partial^2\left[V^{\alpha\beta\gamma} H(f)\right]}{\partial X^\alpha \partial X^\gamma}}_{\text{"Volume source"}} + \underbrace{\frac{\partial\left[S^{\alpha\beta}\delta(f)\right]}{\partial X^\alpha}}_{\text{"Surface source"}} \tag{11}$$

where, $H(f)$ and $\delta(f)$ are respectively the Heaviside unit step function and the Dirac Eq. (1), and they satisfy:

$$H(f) = \begin{cases} 1; & f(x,t) > 0 \\ 0; & f(x,t) < 0 \end{cases}, \ \delta(f) = \frac{dH(f)}{dx}$$

The specific expression of $S^{\alpha\beta}$ is:

$$S^{\alpha\beta} = Q\eta^{\alpha\beta} - Z^{\alpha\beta}(\mathbf{L}, \mathbf{0}) \tag{12}$$

where, $\eta^{\alpha\beta}$ is the metric tensor for flat space-time [10]. The scalar Q and vector L in the dimensionless FW-H equation are respectively the thickness source and load source parameters:

$$Q = N_\gamma \phi^\gamma = \left[\rho\left(u_j - v_j\right) + \rho_0 v_j\right] n_j \tag{13}$$

$$L_i = \left[\rho u_i\left(u_j - v_j\right) + p'\delta_{ij} - \sigma_{ij}\right] n_j \tag{14}$$

Wherein, the thickness source is equivalent to the monopole source noise, usually caused by object movement; the load source is equivalent to dipole noise, usually produced by the sound source on the object surface. Eq. (11) is the four-dimensional FW-H equation established by Dunn [10]. The two terms on the right are respectively referred to as "volume source" and "surface source". However, the extraction of the surface source in Eq. (11) is incomplete, meaning the given surface source term is not the actual surface source term. Combining with numerical prediction research, it's found that there's a significant error. This point will be comparatively analyzed in the third part of the paper. Therefore, corrections must be made.

2.2 Correction of the four-dimensional FW-H equation

The "volume source" term on the right side of Eq. (11) can be expanded as:

$$\frac{\partial^2\left[V^{\alpha\beta\gamma}H(f)\right]}{\partial X^\alpha \partial X^\gamma}=\frac{\partial^2\left[V_1^{\alpha\beta\gamma}H(f)\right]}{\partial X^\alpha \partial X^\gamma}+\frac{\partial}{\partial X^\alpha}\left[H(f)\frac{\partial V_2^{\alpha\beta\gamma}}{\partial X^\gamma}\right]+\frac{\partial}{\partial X^\alpha}\left(V_2^{\alpha\beta\gamma}N_\gamma\delta(f)\right)$$
$$=\frac{\partial^2\left[V_1^{\alpha\beta\gamma}H(f)\right]}{\partial X^\alpha \partial X^\gamma}+\frac{\partial}{\partial X^\alpha}\left(H(f)\frac{\partial V_2^{\alpha\beta\gamma}}{\partial X^\gamma}\right)+\frac{\partial}{\partial X^\alpha}\left(Z^{\alpha\beta}(\mathbf{0},\mathbf{F})\right) \tag{15}$$

where,

$$V_1^{\alpha\beta\gamma}=Z^{\alpha\beta}\left(\mathbf{e}^\gamma,\mathbf{0}\right),\quad V_2^{\alpha\beta\gamma}=Z^{\alpha\beta}\left(\mathbf{0},\mathbf{b}^\gamma\right)$$
$$V_2^{\alpha\beta\gamma}N_\gamma=Z^{\alpha\beta}\left(\mathbf{0},N_\gamma\mathbf{b}^\gamma\right)=Z^{\alpha\beta}\left(\mathbf{0},\mathbf{F}\right) \tag{16}$$

where, the vector is $\boldsymbol{F}=N_\gamma\boldsymbol{b}^\gamma=\boldsymbol{n}\times(\rho\boldsymbol{u})$. For pure acoustic problems, the first two terms on the right side of Eq. (15) are the volume source terms, while the last term is the surface source. If we define:

$$S_C^{\alpha\beta}=S^{\alpha\beta}+Z^{\alpha\beta}\left(\mathbf{0},\mathbf{F}\right) \tag{17}$$

Then, Eq. (11) can be corrected as:

$$\Box^2\left[\phi^\beta H(f)\right]=\underbrace{\frac{\partial^2\left[V_1^{\alpha\beta\gamma}H(f)\right]}{\partial X^\alpha \partial X^\gamma}+\frac{\partial}{\partial X^\alpha}\left[H(f)\frac{\partial V_2^{\alpha\beta\gamma}}{\partial X^\gamma}\right]}_{\text{Volume source}}+\underbrace{\frac{\partial\left[S_C^{\alpha\beta}\delta(f)\right]}{\partial X^\alpha}}_{\text{Surface source}} \tag{18}$$

In practical engineering, the contribution to flow noise mainly comes from the volume source and surface source. Therefore, Table 1 gives a comparative analysis between the correction model in this paper and the four-dimensional sound analogy model of Dunn [10] in terms of their sound source terms. As can be seen from the table, the volume source terms of the two methods are equivalent in both physical meaning and contribution magnitude. However, Dunn's [10] method misses out on the surface source term $\frac{\partial[Z^{\alpha\beta}(\mathbf{0},\boldsymbol{F})\delta(f)]}{\partial X^\alpha}$, and this surface source term is also related to the acoustic velocity vector field. Based on this analysis, it can be deduced that the acoustic velocity vector field obtained by Dunn's [10] method would have errors.

Table 1. Comparison of the corrected four-dimensional FW-H equation with Dunn [10]'s four-dimensional acoustic analogy model

	Volume Source	**Surface Source**
Dunn [10]'s four-dimensional acoustic analogy model	$\frac{\partial^2\left[V^{\alpha\beta\gamma}H(f)\right]}{\partial X^\alpha \partial X^\gamma}$	$\frac{\partial\left[S^{\alpha\beta}\delta(f)\right]}{\partial X^\alpha}$
The corrected four-dimensional FW-H equation	$\frac{\partial^2\left[V_1^{\alpha\beta\gamma}H(f)\right]}{\partial X^\alpha \partial X^\gamma}+\frac{\partial}{\partial X^\alpha}\left[H(f)\frac{\partial V_2^{\alpha\beta\gamma}}{\partial X^\gamma}\right]$	$\frac{\partial\left[S^{\alpha\beta}\delta(f)\right]}{\partial X^\alpha}+\frac{\partial\left[Z^{\alpha\beta}(\mathbf{0},\mathbf{F})\delta(f)\right]}{\partial X^\alpha}$
Difference in the methods	Both have the same physical meaning and contributions	$\frac{\partial\left[Z^{\alpha\beta}(\mathbf{0},\mathbf{F})\delta(f)\right]}{\partial X^\alpha}$

2.3 Four-dimensional acoustic field integral formulation

Considering that the Green's function can describe the propagation law of signals from a point source with unit intensity within the physical space, and this study is based on dimensionless quantities, the dimensionless Green's function [10] is adopted to solve Eqs. (11) and (18). The four-dimensional dimensionless Green's function in the time domain is:

$$G(\mathbf{x},\mathbf{y},t-\tau)=\frac{1}{4\pi}\delta\left(-\frac{1}{2}R^\mu R_\mu\right) \tag{19}$$

where, x and t denote the position and time of the observation point, and y and τ represent the position and time of the sound source. R^μ and R_μ are defined as:

$$R^\mu=\begin{pmatrix}t-\tau\\---\\r_i\end{pmatrix},\ R_\mu=\begin{pmatrix}t-\tau\\---\\-r_i\end{pmatrix},\ r_i=x_i-y_i \tag{20}$$

When the primary aerodynamic sound source is enclosed by the permeable surface, the contribution of the volume integral to the sound field can be neglected, and the noise in the far field can be extrapolated and calculated using only the flow information on the permeable surface. Based on Dunn [10]'s integration method, the semi-analytic integral solutions of Eqs. (11) and (18) can be expressed as:

$$4\pi\phi^\beta(\mathbf{x},t)=\frac{\partial}{\partial X^0}\int_{f=0}\left[\frac{A_\alpha S^{\alpha\beta}}{R_\mu M^\mu}\right]_{\text{ret}}\mathrm{d}\mathbf{y}^2-\int_{f=0}\left[\frac{B_\alpha S^{\alpha\beta}}{R_\mu M^\mu}\right]_{\text{ret}}\mathrm{d}\mathbf{y}^2 \tag{21}$$

and

$$4\pi\phi^\beta(\mathbf{x},t)=\frac{\partial}{\partial X^0}\int_{f=0}\left[\frac{A_\alpha S_C^{\alpha\beta}}{R_\mu M^\mu}\right]_{\text{ret}}\mathrm{d}\mathbf{y}^2-\int_{f=0}\left[\frac{B_\alpha S_C^{\alpha\beta}}{R_\mu M^\mu}\right]_{\text{ret}}\mathrm{d}\mathbf{y}^2 \tag{22}$$

where, $[\cdot]_{\mathrm{ret}}$ denotes the delayed moment value, corresponding to the moment when the sound wave was emitted at the observer's time:

$$A_\alpha = \frac{1}{r}\begin{pmatrix} r \\ ---- \\ -r_i \end{pmatrix}, \quad B_\alpha = \frac{1}{r^2}\begin{pmatrix} 0 \\ ---- \\ r_i \end{pmatrix}, \quad M^\mu = \begin{pmatrix} 1 \\ ---- \\ v_i \end{pmatrix} \tag{23}$$

Detailed derivations of the above equations can be found in Appendix 2.

Converting the derivative of Eq. (21) with respect to the observer's time into a derivative with respect to the sound source's time yields the analytic integral formula:

$$4\pi\phi^\beta(\mathbf{x},t) = \int_{f=0}\left[\frac{rR_\mu M^\mu A_\alpha \dot{S}^{\alpha\beta} + \left(C_\alpha - \left(R_\mu M^\mu\right)^2 B_\alpha\right)S^{\alpha\beta}}{\left(R_\mu M^\mu\right)^3}\right]_{\mathrm{ret}} \mathrm{d}\mathbf{y}^2 \tag{24}$$

where, the dot above the variable denotes differentiation with respect to the sound source's time:

$$C_\alpha = R_\mu M^\mu\left(\dot{R}_\alpha + M_r A_\alpha\right) - R_\alpha \dot{R}_\mu M^\mu - R_\alpha R_\mu \dot{M}^\mu \tag{25}$$

Similarly, the analytic expression for Eq. (22) is:

$$4\pi\phi^\beta(\mathbf{x},t) = \int_{f=0}\left[\frac{rR_\mu M^\mu A_\alpha \dot{S}^{\alpha\beta} + \left(C_\alpha - \left(R_\mu M^\mu\right)^2 B_\alpha\right)S_C^{\alpha\beta}}{\left(R_\mu M^\mu\right)^3}\right]_{\mathrm{ret}} \mathrm{d}\mathbf{y}^2 \tag{26}$$

For clarity, Eqs. (24) and (26) are respectively referred to as T4D and T4DC, where "T" denotes time domain, "4D" stands for four-dimensional, and "C" indicates correction. Therefore, T4D represents the time-domain four-dimensional acoustics calculation Eq. (24), and T4DC signifies the corrected time-domain four-dimensional acoustics calculation Eq. (26). The following section will use T4D and T4DC to compute the development of the far-field four-dimensional acoustic vector over time.

By performing a Fourier transform on both sides of Eqs. (21) and (22), frequency-domain integral formulas can be obtained:

$$\phi^\beta(\mathbf{x},\omega) = \int_{-\infty}^{+\infty}\int_{f=0}\left[\frac{e^{-\mathrm{i}\omega\tau}e^{-\mathrm{i}\omega r}}{4\pi r}\left(\mathrm{i}\omega A_\alpha - B_\alpha\right)S^{\alpha\beta}(\mathbf{y},\tau)\right]_{\mathrm{ret}} \mathrm{d}\mathbf{y}^2\mathrm{d}\tau \tag{27}$$

and

$$\phi^\beta(\mathbf{x},\omega) = \int_{-\infty}^{+\infty}\int_{f=0}\left[\frac{e^{-\mathrm{i}\omega\tau}e^{-\mathrm{i}\omega r}}{4\pi r}\left(\mathrm{i}\omega A_\alpha - B_\alpha\right)S_C^{\alpha\beta}(\mathbf{y},\tau)\right]_{\mathrm{ret}} \mathrm{d}\mathbf{y}^2\mathrm{d}\tau \tag{28}$$

where, i is the imaginary unit, and ω is the dimensionless angular frequency. Eqs. (27) and (28) are named F4D and F4DC respectively, where "F" represents the frequency domain. Thus, F4D represents the frequency-domain four-dimensional acoustics calculation Eq. (27), and F4DC signifies the corrected frequency-domain four-dimensional acoustics calculation Eq. (28). The following section will use F4D and F4DC to compute the development of the far-field four-dimensional acoustic vector with frequency.

For the special case where the permeable surface remains stationary, simplifying the integral formulas can enhance computational efficiency. Under this scenario, distance parameter r, outward normal vector of the permeable surface n, and the sound source's movement speed (equal to zero) v are constants, not depending on the delay time. Moreover, the delay time can be explicitly determined. Therefore, Eqs. (24) and (26) simplify to:

$$4\pi\phi^\beta(\mathbf{x},t) = \int_{f=0}\left[\frac{A_\alpha \dot{S}^{\alpha\beta} - B_\alpha S^{\alpha\beta}}{r}\right]_{\mathrm{ret}} \mathrm{d}\mathbf{y}^2 \tag{29}$$

$$4\pi\phi^\beta(\mathbf{x},t) = \int_{f=0}\left[\frac{A_\alpha \dot{S}_C^{\alpha\beta} - B_\alpha S^{\alpha\beta}}{r}\right]_{\mathrm{ret}} \mathrm{d}\mathbf{y}^2 \tag{30}$$

Eqs. (27) and (28) simplify to:

$$\phi^\beta(\mathbf{x},\omega) = \int_{f=0}\frac{e^{-\mathrm{i}\omega r}}{4\pi r}\left(\mathrm{i}\omega A_\alpha - B_\alpha\right)S^{\alpha\beta}(\mathbf{y},\omega)\mathrm{d}\mathbf{y}^2 \tag{31}$$

$$\phi^\beta(\mathbf{x},\omega) = \int_{f=0}\frac{e^{-\mathrm{i}\omega r}}{4\pi r}\left(\mathrm{i}\omega A_\alpha - B_\alpha\right)S_C^{\alpha\beta}(\mathbf{y},\omega)\mathrm{d}\mathbf{y}^2 \tag{32}$$

It's worth noting that formulas T4DC and F4DC only correct the source terms of three components of the acoustic velocity in the four-dimensional variable ϕ^β. Furthermore, for linear small-amplitude fluctuations, the acoustic density ρ' is much smaller than the uniform average inflow density ρ_0, so the $\rho\boldsymbol{u} \approx \boldsymbol{u}$ holds true.

3. NUMERICAL VERIFICATION AND ANALYSIS

Examples of point source radiation are commonly used for numerical validation of aeroacoustic theoretical formulas. Consider the sound radiation from a stationary dipole with self-excited angular frequency $\omega_s = 3$ and a rotating monopole, in order to focus on the acoustic velocity formula and avoid any deviations related to the accuracy of flow simulation, transient flow parameters on the permeable surface, including pressure, density, and velocity, are generated by the exact solution of the flow field produced by the point source. In the four-dimensional time domain integration formula, the time derivative is approximated using a fourth-order finite difference method, and the acoustic signal at the observation point is calculated using the advanced time algorithm [23]. The analysis is conducted from three perspectives: time domain, frequency domain, and spatial domain. The specific steps of the numerical prediction are shown in the flowchart in Figure 1.

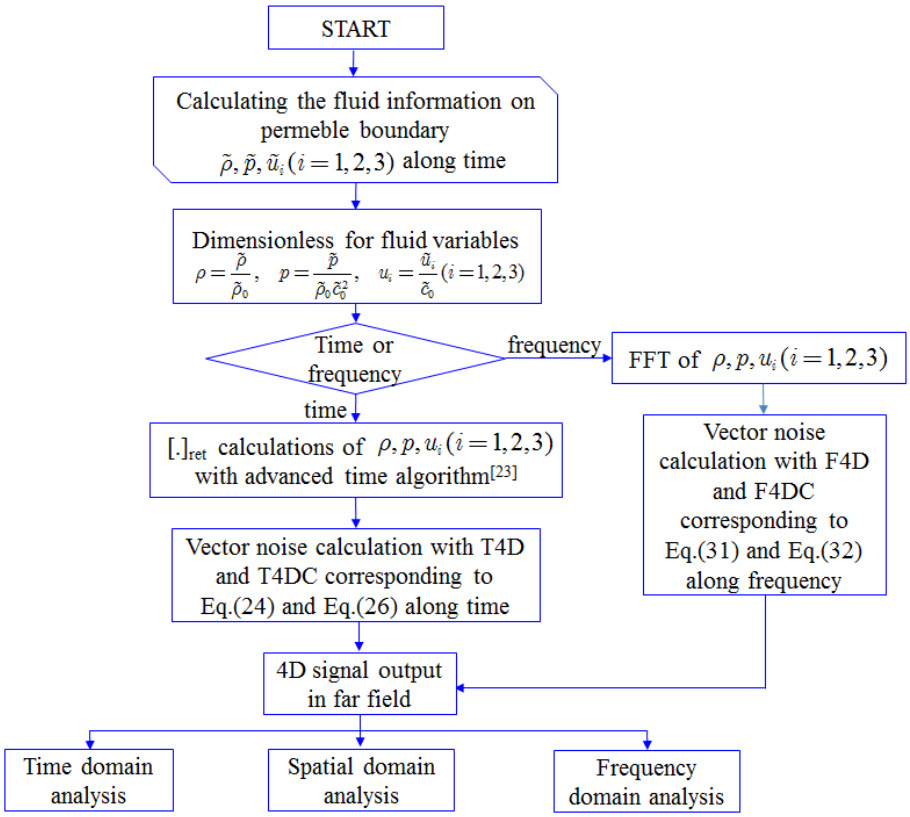

Figure 1. Flowchart of the four-dimensional vector noise algorithm

3.1 Stationary dipole

Consider the sound radiation from a stationary dipole. Assume that the dipole is located at the origin of the coordinate system, with its axis aligned with x_2 axis. The dimensionless velocity potential function of the dipole's sound field can be represented as:

$$\phi(\mathbf{x},t)=\frac{\partial}{\partial x_2}\left\{\frac{A}{4\pi r}\exp\left[\mathrm{i}\omega\left(t-r\right)\right]\right\} \tag{33}$$

where, A represents the amplitude of the velocity potential function, and $r=|\boldsymbol{x}-y|$ is the acoustic radius. The corresponding acoustic velocity, pressure, and density fields can be expressed as:

$$\begin{aligned} &u_i(\mathbf{x},t)=\frac{\partial\phi(\mathbf{x},t)}{\partial x_i},\ p'(\mathbf{x},t)=-\frac{\partial\phi(\mathbf{x},t)}{\partial t} \\ &\rho'(\mathbf{x},t)=p'(\mathbf{x},t) \end{aligned} \tag{34}$$

A cube with a center at the coordinate origin and a side length of 1 was taken as the permeable surface. This surface was discretized into an integral surface using a structured grid of 9600 cells to ensure spatial resolution accuracy. 128 time steps were set within each sound source period to guarantee the numerical accuracy of the difference algorithm. 120 observation points were evenly distributed on a circle with a radius of 20 in the x_1-x_2 plane, with the geometric angle between the observation point measured based on the x_1 axis and the origin defined as the observation angle θ.

(1) Time-domain noise signal

The sound pressure and acoustic velocity radiated by the dipole were calculated using the time-domain formulas T4D and T4DC. To visually display the sound field, a flow characteristic length of 1m was chosen. The density of the medium in equilibrium was 1.2kg/m^3, and the speed of sound was c_0=340m/s. The numerical results were converted into dimensional parameters for output. For this case, the amplitude of the velocity potential function was A=1/c_0. Figure 2 displays the change of the sound field with time at different observation angles, and its comparison with the exact solution. The sound pressure numerical solutions obtained by formulas T4D and T4DC are in complete agreement with the exact solution. The acoustic velocity numerical results from formula T4DC are consistent with the theoretical solution, but the magnitude and phase of the acoustic velocity predicted by formula T4D show noticeable differences from the theoretical solution. This discrepancy is due to the loss of some effective sound sources on the permeable surface. By changing the self-excited frequency of the point source or the size of the permeable surface, formula T4DC always produces results that are in full agreement with the theoretical solution.

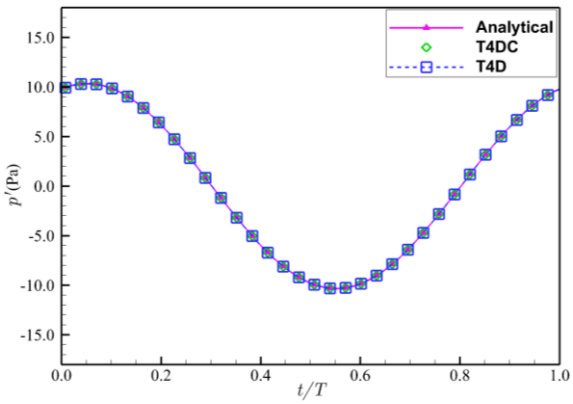

(*a*) Sound pressure

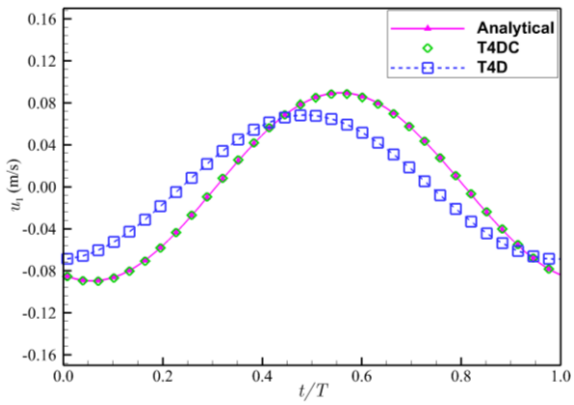

(b) Acoustic velocity in direction x_1

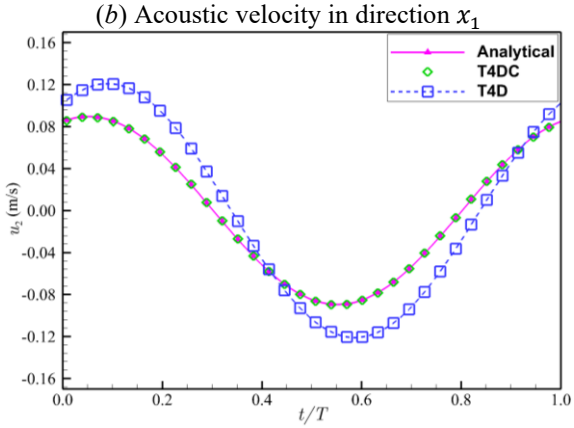

(c) Acoustic velocity in direction x_2

Figure 2. Time history of sound pressure and acoustic velocity signals from a stationary dipole at $\theta = 135^{\circ}$ observation angle

(2) Frequency-domain noise signal

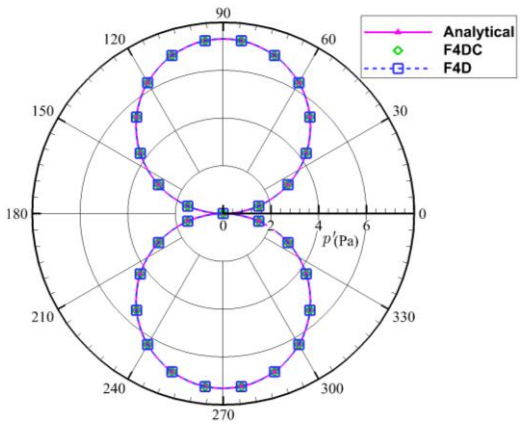

(a) Acoustic pressure directivity

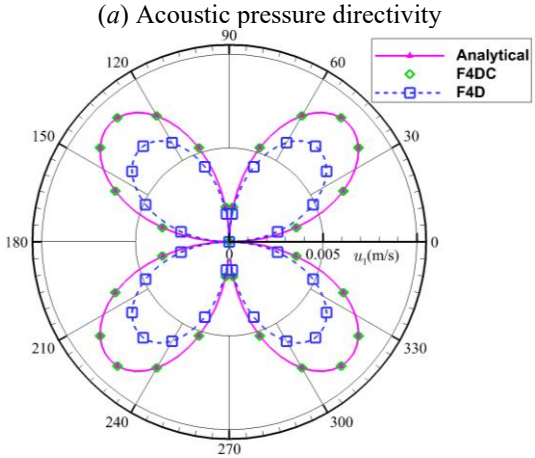

(b) Directionality of acoustic velocity in direction x_1

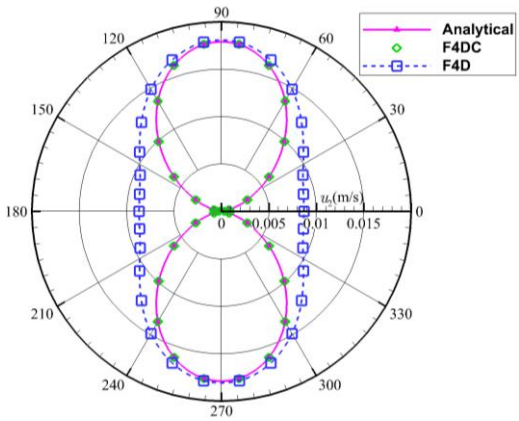

(c) Directionality of acoustic velocity in direction x_2

Figure 3. Directionality distribution of sound pressure and acoustic velocity signals from a stationary dipole

The sound pressure and acoustic velocity radiated by the dipole were calculated using the frequency-domain formulas F4D and F4DC. Figure 3 presents the directivity distribution of the sound field under the dipole's self-excited frequency and its comparison with the exact solution. The acoustic velocity numerical solution of formula F4DC is highly consistent with the theoretical solution, while the acoustic velocity numerical solution of formula F4D shows significant differences from the theoretical solution. Such a discrepancy is anticipated. As previously mentioned, formula F4DC does not change the sound pressure source term in formula F4D. Therefore, the sound pressure numerical solutions of formulas F4D and F4DC are identical and are in full agreement with the exact solution. This indicates that the source term used to calculate sound pressure in formula F4DC is correct.

3.2 Rotating monopole

Assuming a monopole with an initial azimuthal angle of 0° rotates counterclockwise around the x_3 axis at a constant angular velocity $\omega_r = \frac{\omega_s}{4}$ with a rotation radius $r_a = 0.25$. The self-excited frequency of the monopole, the amplitude of the velocity potential function, as well as the permeable surface grid and observation point positions, are the same as those in the stationary dipole case. The dimensionless velocity potential function of the monopole is given by:

$$\phi(\mathbf{x},t) = \frac{A}{4\pi r(1-M_r)} \exp\left[\mathrm{i}\omega(t-r)\right] \tag{35}$$

where, M_r is the Mach number of the monopole moving towards the observation point at the delayed moment and is defined as $M_r = \frac{r_j v_j}{r}$. The acoustic velocity, pressure, and density fields induced by the monopole are obtained from Eq. (34).

(1) Time-domain noise signal

Using the time-domain formulas T4D and T4DC, the sound pressure and acoustic velocity radiated by the rotating monopole were calculated. Figure 4 illustrates the variation of the sound field at the observation angle $\theta = 135^{\circ}$ over time and its comparison with the precise solution. Once again, the sound pressure and acoustic velocity predicted by formula T4DC are consistent with the theoretical solution, while formula T4D only has the sound pressure numerical solution

matching the precise solution, and there is a certain difference in the acoustic velocity numerical result from the theoretical solution. Compared to the stationary dipole case, the error in the acoustic velocity of the rotating monopole calculated by formula T4D is smaller. This is because the permeable surface source term lost in formula T4D belongs to the load source. Figure 5 further provides the spatial directionality distribution of the root mean square (RMS) value of the acoustic velocity. At all observation points, the acoustic velocity predicted by formula T4DC is consistent with the precise solution, while there is a difference between the numerical solution of formula T4D and the precise solution.

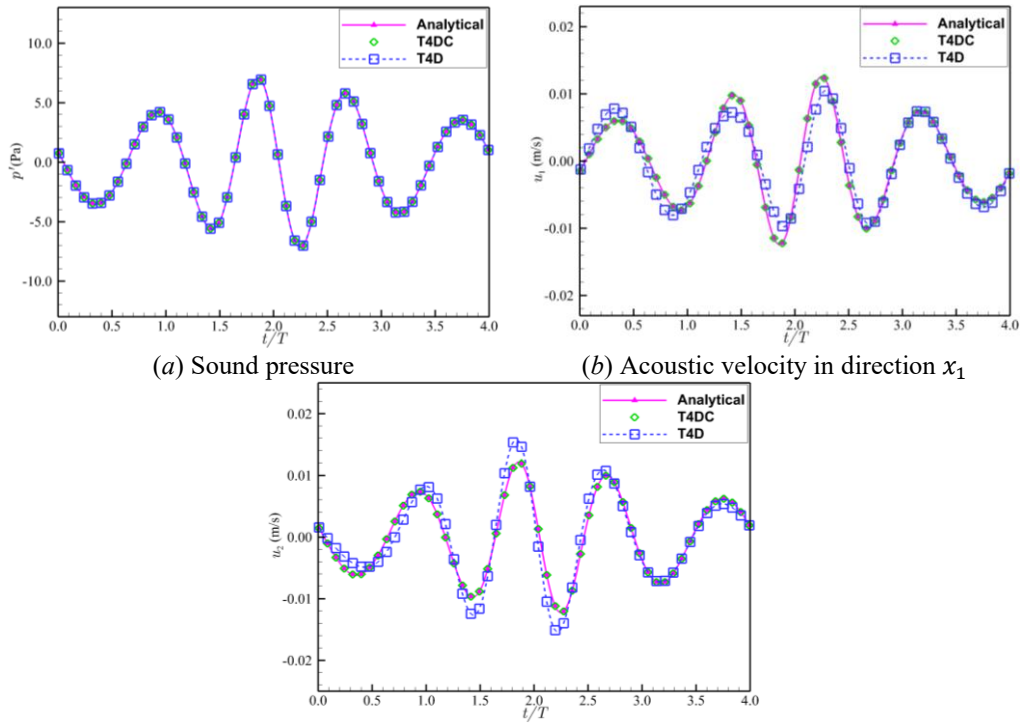

(a) Sound pressure (b) Acoustic velocity in direction x_1

(c) Acoustic velocity in direction x_2

Figure 4. Time history of sound pressure and acoustic velocity signals from a rotating monopole at $\theta = 135^{\circ}$observation angle

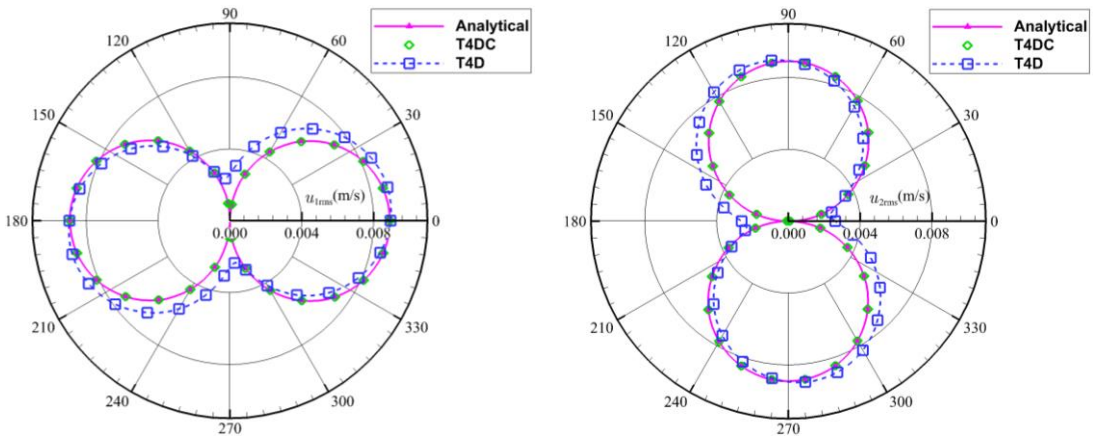

(a) Acoustic velocity in direction x_1 (b) Acoustic velocity in direction x_2

Figure 5. Directionality distribution of the RMS value of the acoustic velocity signal from the rotating monopole

(2) Frequency-domain noise signal

The frequency-domain formulas F4D and F4DC were used to calculate the sound field radiated by the moving monopole. The rotation of the sound source induces a Doppler frequency domain phenomenon, causing the acoustic signal received at the observation point to be distributed over a series of discrete frequencies. The corresponding angular frequencies satisfy a mathematical relationship $\omega = \omega_s + m\omega_r$, where m=0,1,2... represents the harmonic order. Figure 6 presents the predicted results of the sound field spectrum at an observation angle $\theta = 135^{\circ}$ and their comparison with the precise solution. The figure indicates that the energy of the sound wave is mainly concentrated on five frequencies around $m = -1, 0, 1, 2, 3$. As the frequency increases, the sound pressure and acoustic velocity predicted by formula F4DC remain consistent with the theoretical solution. Figure 6(a) shows that the sound pressure amplitude obtained by formula F4D aligns with the precise solution. In contrast, Figures 6(b)-(c) depict that the acoustic velocity numerical results from formula F4D only match the theoretical solution at frequency $m = 0$; there are significant differences at other frequencies. Taking the velocity component in the x_1 direction as an example, the relative error of F4D reaches 25.5% at frequency $m = -1$ and astonishingly 35.8% at frequency $m = 1$. Meanwhile, the

velocity component in the $x_2$direction has relative errors of 38.6% and 61.1% at frequencies $m = 1$ and $m = 2$ respectively. To clarify the effect of harmonic frequency on acoustic velocity, Figure 7 presents the directionality distribution of the acoustic velocity predicted by formulas T4D and T4DC at frequency $m = 1$. Clearly, for observation points in different angular directions, formula T4DC achieves predictions consistent with the precise solution, while the directionality prediction of formula T4D deviates by approximately 25° from the precise solution. It's evident that the directional deviation caused by harmonic frequency is actually due to the change in angle, which naturally causes a change in the amplitude of the sound wave, explaining the amplitude deviation of the acoustic velocity at the harmonic frequencies shown in Figures 6(b)-(c).

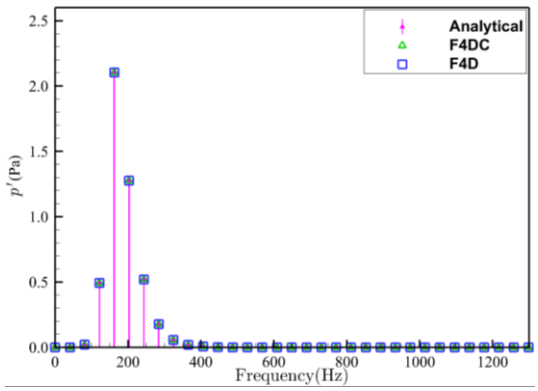

(a) Sound pressure

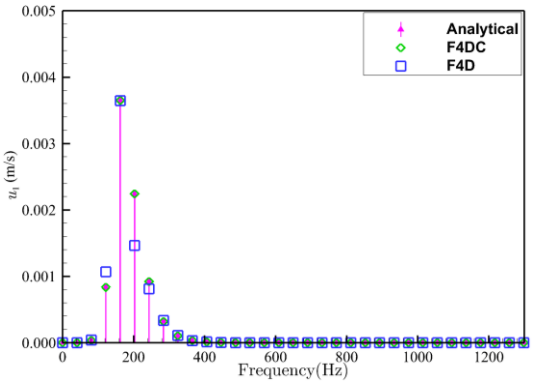

(b) Acoustic velocity in direction x_1

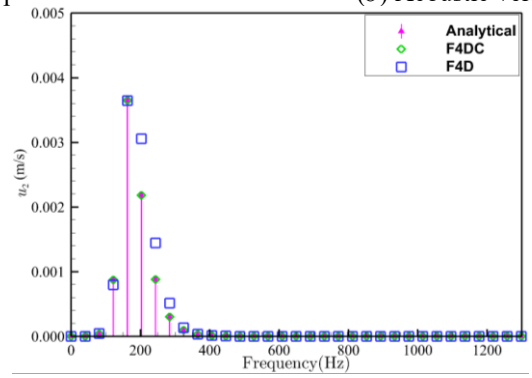

(c) Acoustic velocity in direction x_2

Figure 6. Spectrum of rotating monopole acoustic pressure and acoustic velocity signals at the $\theta = 135^{\circ}$ observation angle

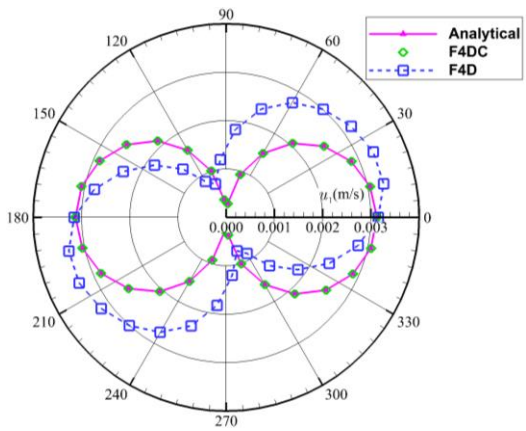

(a) Acoustic velocity in direction x_1

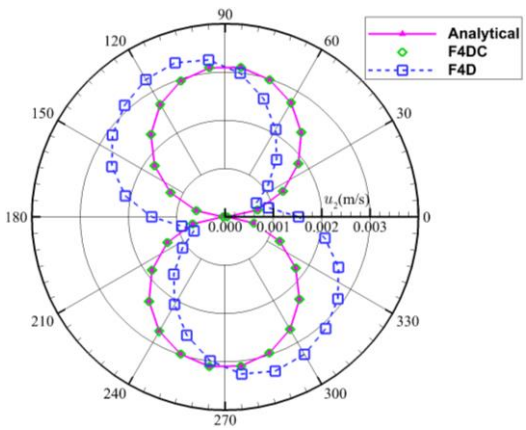

(b) Acoustic velocity in direction x_2

Figure 7. Directionality distribution of the acoustic velocity signal of the rotating monopole at frequency $\omega = \omega_s + \omega_r$

Further examination was made on the spatial distribution characteristics of the sound field of the rotating monopole. As inferred from Figure 6, the peak value of the sound field occurs at the frequency corresponding to $m = 0$. Figure 8 presents the amplitude and real part contour plots of the sound pressure and acoustic velocity calculated by formula T4DC at this frequency. As observed from Figure 8, no Doppler effect of the sound field exists at $m = 0$. The amplitude and real part of the sound pressure propagate outwards in a typical concentric circle uniform radiation pattern. The sound pressure amplitude on these concentric circles is the same and is independent of the angle corresponding to the observation point. The amplitude and real parts of the acoustic velocity components u_1 and u_2 respectively display a horizontal figure-eight and a vertical figure-eight typical dipole radiation pattern. This is consistent with the theoretical solution given by formulas (34)-

(35). Combining with the theoretical solution, it's known that the acoustic velocity in the monopole x_2 direction spatially equates to the pressure field of the dipole. As a result, the acoustic velocity component u_2 appears as a vertical distribution shaped as the number 8 that is consistent with Figure 2(a). Simultaneously, the acoustic velocity u_1 displays a distribution perpendicular to u_2, naturally manifesting as a horizontal 8-shaped pattern.

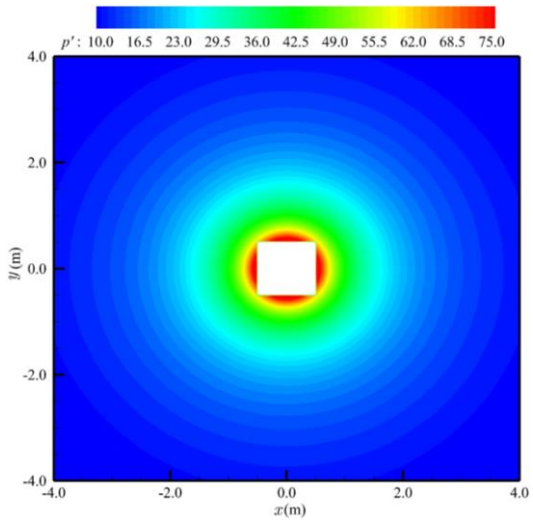

(a) Spatial distribution of acoustic pressure amplitude

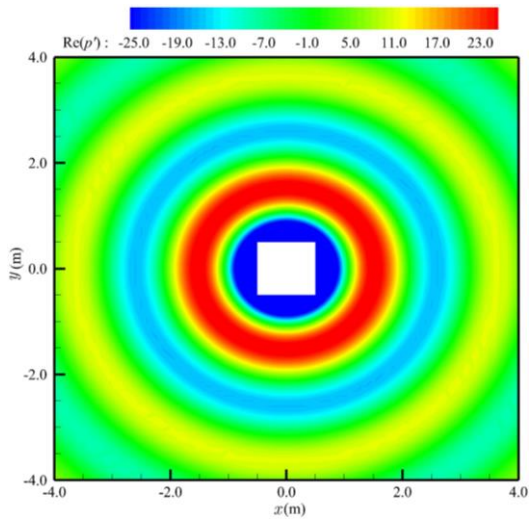

(b) Spatial distribution of the real part of acoustic pressure

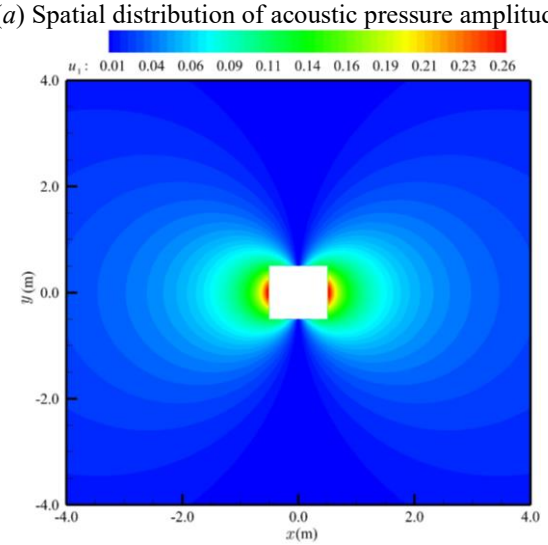

(c) Spatial distribution of acoustic velocity amplitude in direction x_1

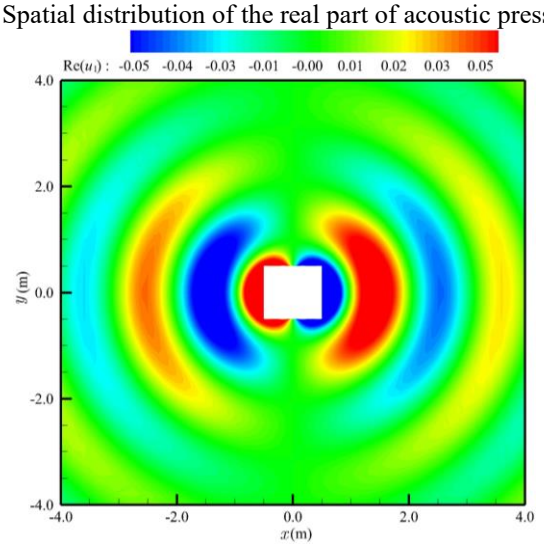

(d) Spatial distribution of the real part of acoustic velocity in direction x_1

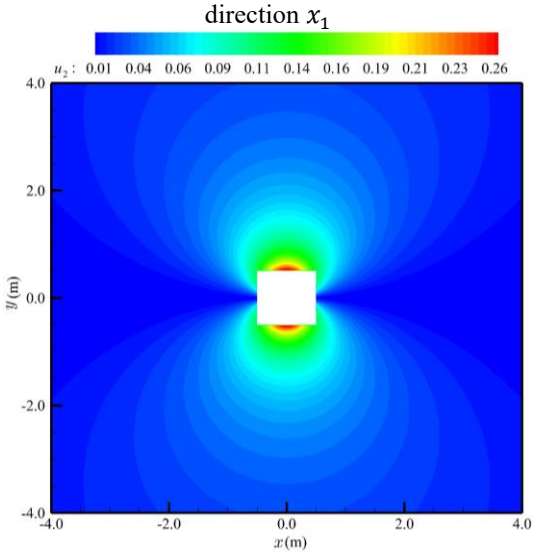

(e) Spatial distribution of acoustic velocity amplitude in direction x_2

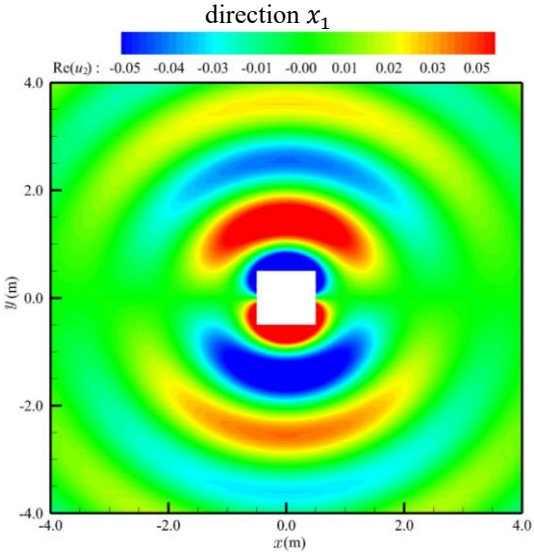

(f) Spatial distribution of the real part of acoustic velocity in direction x_2

Figure 8. Cloud maps of the amplitude and real part spatial distribution of the sound pressure and acoustic velocity signal of the rotating monopole at frequency $\omega = \omega_s$

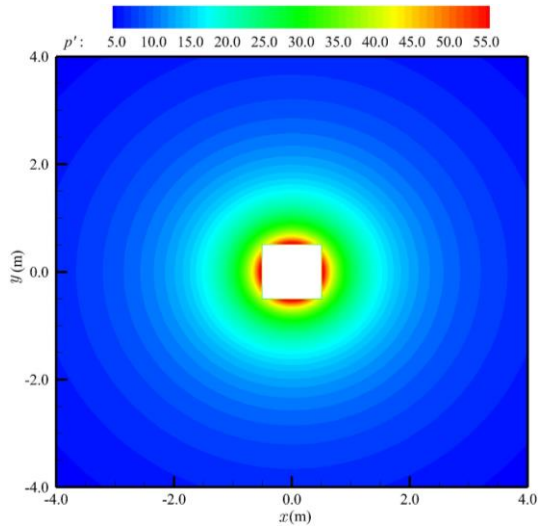

(*a*) Spatial distribution of acoustic pressure amplitude

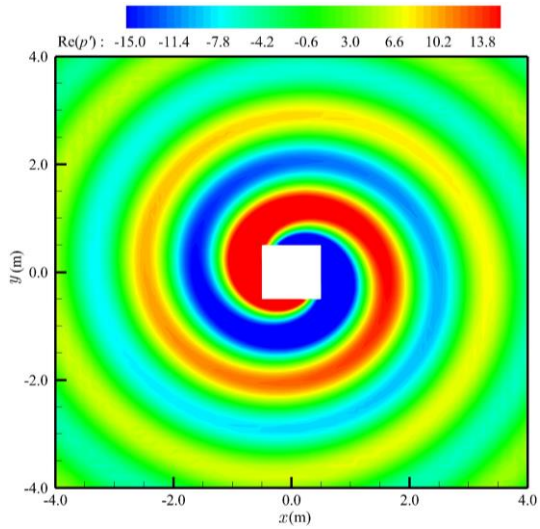

(*b*) Spatial distribution of the real part of acoustic pressure

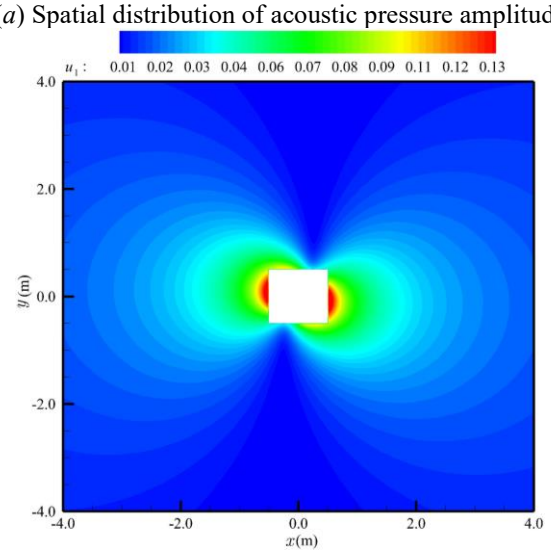

(*c*) Spatial distribution of acoustic velocity amplitude in direction x_1

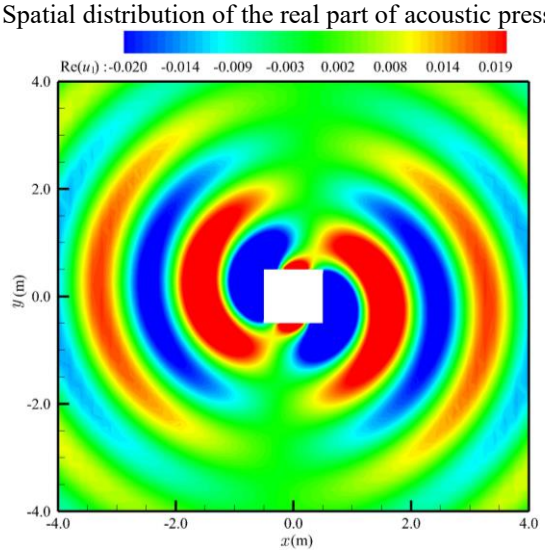

(*d*) Spatial distribution of the real part of acoustic velocity in direction x_1

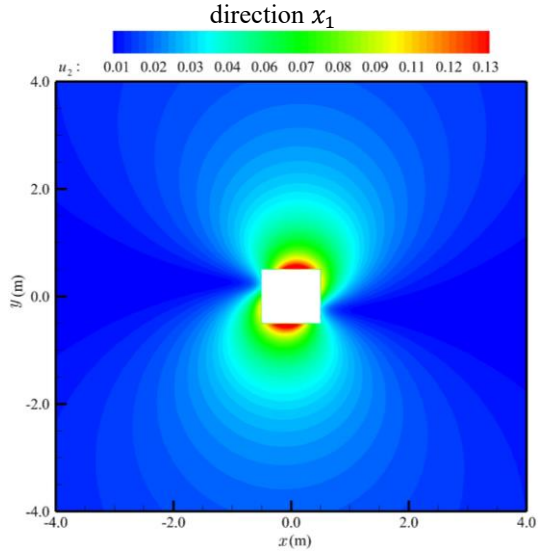

(*e*) Spatial distribution of acoustic velocity amplitude in direction x_2

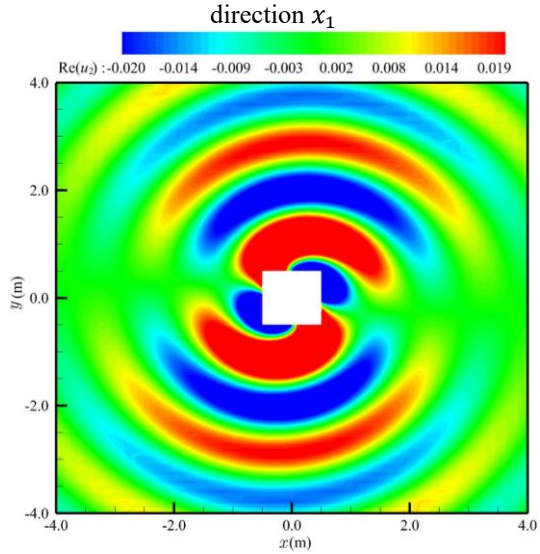

(*f*) Spatial distribution of the real part of acoustic velocity in direction x_2

Figure 9. Cloud maps of the amplitude and real part spatial distribution of the sound pressure and acoustic velocity signal of the rotating monopole at frequency $\omega = \omega_s + \omega_r$

Figure 9 presents the amplitude and real part contour plots of the sound pressure and acoustic velocity predicted by formula T4DC at frequency $m = 1$. At this time, the Doppler effect of sound propagation is observed. Both the real parts of sound pressure and acoustic velocity radiate outwards in a spiral manner. While the amplitude of the sound pressure still follows a concentric circle uniform radiation pattern, the distribution of the amplitude of the acoustic velocity shows an

approximate 25° deflection, with positive and negative values alternating. Influenced by the real part component, both the sound pressure amplitude and the acoustic velocity display similar spatial distributions. The amplitude of sound pressure exhibits a standard concentric circle distribution, showing a gradual linear decline during propagation and appearing as a strong sound field near the permeable surface, with the amplitude decreasing as the distance increases. The real part of the acoustic velocity in the spatial domain manifests as a 25° deflected spiral, thus the amplitudes of acoustic velocity in the x_1 and x_2 directions each display a horizontal or vertical oblique dipole distribution. Moreover, affected by the harmonic order, Figure 9 exhibits a spatial distribution different from Figure 8. Therefore, it can be inferred that the harmonic order is the cause of the sound field's 25° directional deflection, and as the harmonic order increases, the angle of the directional deflection accumulates. However, in conjunction with Figure 7, the energy concentrated by the high-order harmonics of $m > 2$ barely affects the overall distribution of the sound field, and the energy concentrated by the harmonic components of $m = 2$ is much less than that of $m = 1$, hence the influence of harmonics of $m > 2$ is disregarded. Combining the above analyses, it can be determined that the harmonic components are the reason for the non-periodic distribution of noise from the rotating monopole.

4. CONCLUSION

The four-dimensional acoustic analogy formula proposed by Dunn [10] faces challenges in accurately predicting the propagation of acoustic velocity due to incomplete extraction of the integral surface load source term. By extracting the complete permeable load source, this study developed the time-domain integral analytical formula T4DC and the frequency-domain integral analytical formula F4DC. These formulas aim to compute the sound pressure and acoustic velocity field predictions in a static medium. The main conclusions are:

(1) The effectiveness of formulas T4DC and F4DC and their implementations have been strongly demonstrated through typical test cases of stationary dipoles and rotating monopoles. Both test cases utilized permeable data surfaces, and the flow parameters on these permeable surfaces were obtained from the exact solution of the flow field generated by a point source. The numerical prediction results of T4DC and F4DC are very consistent with the exact solutions, indicating that the method proposed in this study can capture multi-domain features of vector noise in time, frequency, and spatial domains.

(2) The far-field signal of a stationary dipole source exhibits a periodic distribution over time, consistent with the physical characteristics of sound propagation. Within the frequency domain, both the dipole and the y-direction velocity components show a standard distribution shaped as 8, while the x-direction velocity displays a standard quadripole petal-shaped distribution. In contrast, the far-field signal of a rotating monopole shows non-periodic fluctuations over time. The amplitude of the far-field vector signal shows a trend of first increasing and then gradually decreasing with frequency, and it is concentrated only at certain discrete frequencies. In the spatial domain, the vector acoustic field distribution of a rotating monopole is significantly influenced by the harmonic order.

(3) It's worth noting that formulas T4DC and F4DC are only applicable for predicting sound pressure and acoustic velocity signals in a static medium. Future work will focus on developing new four-dimensional acoustic analogy formulas suitable for moving media. Since the flow equation for a stationary medium is analogous to the Maxwell equation for stationary magnetofluid, it can be directly combined with concepts such as fluid electric and magnetic fields to establish vector equations. The physical equations for moving media differ from those for stationary media. Building upon the research foundation of this paper, it will be necessary to reconstruct the acoustic analogy equations and then carry out theoretical and numerical prediction studies.

ACKNOWLEDGMENT

The research was supported by the research project of the National Key Laboratory of Science and Technology on Aerodynamic Design and Research (no. 614220120030115) and the Natural Science Foundation of Ningxia (no. 2021AAC03209).

REFERENCES

[1] Williams, J.F., Hawkings, D.L. (1969). Sound generation by turbulence and surfaces in arbitrary motion. Philosophical Transactions for the Royal Society of London. Series A, Mathematical and Physical Sciences, 264(1151): 321-342. https://www.jstor.org/stable/73790.

[2] Di Francescantonio, P. (1997). A new boundary integral formulation for the prediction of sound radiation. Journal of Sound and Vibration, 202(4): 491-509. https://doi.org/10.1006/jsvi.1996.0843

[3] Zhong, S., Zhang, X. (2017). A sound extrapolation method for aeroacoustics far-field prediction in presence of vortical waves. Journal of Fluid Mechanics, 820: 424-450. https://doi.org/10.1017/jfm.2017.219

[4] Farassat, F. (2007). Derivation of Formulations 1 and 1A of Farassat (No. L-19318). NASA Technical Report TM-2007-214853, 2007.

[5] Jacobsen, F. (1991). A note on instantaneous and time-averaged active and reactive sound intensity. Journal of Sound and Vibration, 147(3): 489-496. https://doi.org/10.1016/0022-460X(91)90496-7

[6] Gennaretti, M., Testa, C. (2008). A boundary integral formulation for sound scattered by elastic moving bodies. Journal of Sound and Vibration, 314(3-5): 712-737. https://doi.org/10.1016/j.jsv.2008.01.028

[7] Gennaretti, M., Bernardini, G., Poggi, C., Testa, C. (2018). Velocity-potential boundary-field integral formulation for sound scattered by moving bodies. AIAA Journal, 56(9): 3547-3557. https://doi.org/10.2514/1.J056491

[8] Lee, S., Brentner, K.S., Morris, P.J. (2011). Assessment of time-domain equivalent source method for acoustic scattering. AIAA Journal, 49(9): 1897-1906. https://doi.org/10.2514/1.J050736

[9] Crocker, M.J., Jacobsen, F. (2007). Sound Intensity. Encyclopedia of Acoustics, Volume Four, Wiley Publication.

[10] Dunn, M.H. (2019). The acoustic analogy in four dimensions. International Journal of Aeroacoustics,

18(8): 711-751. https://doi.org/10.1177/1475472X19890259
[11] Farassat, F., Brentner, K.S. (2005). The derivation of the gradient of the acoustic pressure on a moving surface for application to the Fast Scattering Code (FSC) (No. NASA/TM-2005-213777).
[12] Lee, S., Brentner, K.S., Farassat, F., Morris, P.J. (2009). Analytic formulation and numerical implementation of an acoustic pressure gradient prediction. Journal of Sound and Vibration, 319(3-5): 1200-1221. https://doi.org/10.1016/j.jsv.2008.06.028
[13] Lee, S., Brentner, K.S., Morris, P.J. (2012). Time-domain approach for acoustic scattering of rotorcraft noise. Journal of the American Helicopter Society, 57(4): 1-12. https://doi.org/10.4050/JAHS.57.042001
[14] Ghorbaniasl, G., Carley, M., Lacor, C. (2013). Acoustic velocity formulation for sources in arbitrary motion. AIAA Journal, 51(3): 632-642. https://doi.org/10.2514/1.J051958
[15] Mao, Y., Zhang, Q., Xu, C., Qi, D. (2015). Two types of frequency-domain acoustic-velocity formulations for rotating thickness and loading sources. AIAA Journal, 53(3): 713-722. https://doi.org/10.2514/1.J053230
[16] Mao, Y., Xu, C., Qi, D. (2015). Computation of instantaneous and time-averaged active acoustic intensity field around rotating source. Journal of Sound and Vibration, 337: 95-115. https://doi.org/10.1016/j.jsv.2014.10.023
[17] Mao, Y., Gu, Y., Xu, C. (2016). Validation of frequency-domain method to compute noise radiated from rotating source and scattered by surface. AIAA Journal, 54(4): 1188-1197. https://doi.org/10.2514/1.J053674
[18] Mao, Y., Tang, H., Xu, C. (2016). Vector wave equation of aeroacoustics and acoustic velocity formulations for quadrupole source. AIAA Journal, 54(6): 1922-1931. https://doi.org/10.2514/1.J054687
[19] Lee, S., Brentner, K.S. (2016). Comment on "acoustic velocity formulation for sources in arbitrary motion". AIAA Journal, 54(5): 1810-1811. https://doi.org/10.2514/1.J054845
[20] He, J., Xue, S., Liu, Q., Yang, D., Wang, L. (2022). Acoustic velocity analogy formulation for sources in quiescent medium. Proceedings of the Institution of Mechanical Engineers, Part G: Journal of Aerospace Engineering, 237(13): 3018-3031. https://doi.org/10.1177/09544100231174332
[21] Kambe, T. (2010). A new formulation of equations of compressible fluids by analogy with Maxwell's equations. Fluid Dynamics Research, 42(5): 055502. https://doi.org/10.1088/0169-5983/42/5/055502
[22] Najafi-Yazdi, A., Brès, G.A., Mongeau, L. (2011). An acoustic analogy formulation for moving sources in uniformly moving media. Proceedings of the Royal Society A: Mathematical, Physical and Engineering Sciences, 467(2125): 144-165. https://doi.org/10.1098/rspa.2010.0172
[23] Casalino, D. (2003). An advanced time approach for acoustic analogy predictions. Journal of Sound and Vibration, 261(4): 583-612. https://doi.org/10.1016/S0022-460X(02)00986-0

APPENDIX

1. Dimensionless definition

Considering the propagation of sound waves in a uniform and stationary medium, the local pressure $\tilde{p}$, density $\tilde{\rho}$, and velocity of the fluid $\tilde{u}$ are decomposed into a uniform field and small disturbances:

$$\tilde{p}=\tilde{p}_0+\tilde{p}',\quad \tilde{\rho}=\tilde{\rho}_0+\tilde{\rho}',\quad \tilde{\mathbf{u}}=\tilde{\mathbf{u}}' \tag{A1}$$

where, $\tilde{\rho}_0$ and $\tilde{p}_0$ represent the average density and average pressure of the uniform field; small disturbances $\tilde{p}'$, $\tilde{\rho}'$ and $\tilde{u}'$ are the acoustic pressure, acoustic density, and acoustic velocity, respectively. Assuming the characteristic size of the flow is $\tilde{L}_0$, the spatial variable $\tilde{u}$, time variable $\tilde{t}$, and flow parameters are rendered dimensionless as:

$$\mathbf{x}=\frac{\tilde{\mathbf{x}}}{\tilde{L}_0},\quad t=\frac{\tilde{c}_0\tilde{t}}{\tilde{L}_0} \tag{A2}$$

$$\rho=\frac{\tilde{\rho}}{\tilde{\rho}_0},\quad p=\frac{\tilde{p}}{\tilde{\rho}_0\tilde{c}_0^2},\quad \mathbf{u}=\frac{\tilde{\mathbf{u}}}{\tilde{c}_0},\quad \sigma_{ij}=\frac{\tilde{\sigma}_{ij}}{\tilde{\rho}_0\tilde{c}_0^2} \tag{A3}$$

By combining the above dimensionless definitions, we can get Eqs. (1)-(3).

2. Derivation of delayed time acoustic vector integral Eqs. (21)-(22)

By combining the dimensionless Green's function expression (19), the solutions of Eqs. (11) and (18) can be expressed as:

$$\phi^{\beta}(\mathbf{x},t)=\frac{\partial}{\partial X^{\alpha}}\int_{-\infty}^{+\infty}\int_{f=0}G(\mathbf{x},\mathbf{y},t-\tau)S^{\alpha\beta}(\mathbf{y},\tau)\mathrm{d}\mathbf{y}^2\mathrm{d}\tau \tag{A4}$$

$$\phi^{\beta}(\mathbf{x},t)=\frac{\partial}{\partial X^{\alpha}}\int_{-\infty}^{+\infty}\int_{f=0}G(\mathbf{x},\mathbf{y},t-\tau)S_C^{\alpha\beta}(\mathbf{y},\tau)\mathrm{d}\mathbf{y}^2\mathrm{d}\tau \tag{A5}$$

The partial derivative components of the first-order tensor in the above equations contain partial derivatives concerning time and partial derivatives concerning the three spatial components. Generally, the partial derivatives concerning space can be transformed into partial derivatives concerning time [23]. At the same time, combined with the partial derivative relationship proposed by Dunn [10]:

$$\frac{\partial G(\mathbf{x},t;\mathbf{y},\tau)}{\partial X^{\alpha}}=\frac{\partial A_{\alpha}G}{\partial X^{0}}-B_{\alpha}G(\mathbf{x},t;\mathbf{y},\tau) \tag{A6}$$

The above two equations can be simplified as:

$$\begin{aligned}\phi^{\beta}(\mathbf{x},t)=&\frac{\partial}{\partial X^{0}}\int_{-\infty}^{+\infty}\int_{f=0}G(\mathbf{x},\mathbf{y},t-\tau)A_{\alpha}S^{\alpha\beta}(\mathbf{y},\tau)\mathrm{d}\mathbf{y}^2\mathrm{d}\tau\\&-\int_{-\infty}^{+\infty}\int_{f=0}G(\mathbf{x},\mathbf{y},t-\tau)B_{\alpha}S^{\alpha\beta}(\mathbf{y},\tau)\mathrm{d}\mathbf{y}^2\mathrm{d}\tau\end{aligned} \tag{A7}$$

$$\phi^{\beta}(\mathbf{x},t)= \frac{\partial}{\partial X^{0}}\int_{-\infty}^{+\infty}\int_{f=0} G(\mathbf{x},\mathbf{y},t-\tau)A_{\alpha}S_{C}^{\alpha\beta}(\mathbf{y},\tau)\mathrm{d}\mathbf{y}^{2}\mathrm{d}\tau -\int_{-\infty}^{+\infty}\int_{f=0} G(\mathbf{x},\mathbf{y},t-\tau)B_{\alpha}S_{C}^{\alpha\beta}(\mathbf{y},\tau)\mathrm{d}\mathbf{y}^{2}\mathrm{d}\tau \tag{A8}$$

where,

$$A_{\alpha}=\frac{1}{t-\tau}\begin{pmatrix} t-\tau \\ ---- \\ -r_i \end{pmatrix} B_{\alpha}=\frac{1}{(t-\tau)^{2}}\begin{pmatrix} 0 \\ ---- \\ r_i \end{pmatrix} \tag{A9}$$

According to the integral formulas in references [10, 22], the above double integral expressions can be simplified to a relationship concerning boundary integration at a delayed time, namely Eqs. (21) and (22)

$$4\pi\phi^{\beta}(\mathbf{x},t)=\frac{\partial}{\partial X^{0}}\int_{f=0}\left[\frac{A_{\alpha}S^{\alpha\beta}}{R_{\mu}M^{\mu}}\right]_{\mathrm{ret}}\mathrm{d}\mathbf{y}^{2} -\int_{f=0}\left[\frac{B_{\alpha}S^{\alpha\beta}}{R_{\mu}M^{\mu}}\right]_{\mathrm{ret}}\mathrm{d}\mathbf{y}^{2} \tag{A10}$$

$$4\pi\phi^{\beta}(\mathbf{x},t)=\frac{\partial}{\partial X^{0}}\int_{f=0}\left[\frac{A_{\alpha}S_{C}^{\alpha\beta}}{R_{\mu}M^{\mu}}\right]_{\mathrm{ret}}\mathrm{d}\mathbf{y}^{2} -\int_{f=0}\left[\frac{B_{\alpha}S_{C}^{\alpha\beta}}{R_{\mu}M^{\mu}}\right]_{\mathrm{ret}}\mathrm{d}\mathbf{y}^{2} \tag{A11}$$

where, $[\cdot]_{\mathrm{ret}}$ represents the value at a delayed time. As can be seen from Eq. (6), in fact, $\frac{\partial}{\partial X^{0}}=\frac{\partial}{\partial t}$. Taking Eq. (22) as an example, the first term on the right side of the equation can be expressed as:

$$\begin{aligned}\frac{\partial}{\partial X^{0}}\int_{f=0}\left[\frac{A_{\alpha}S_{C}^{\alpha\beta}}{R_{\mu}M^{\mu}}\right]_{\mathrm{ret}}\mathrm{d}\mathbf{y}^{2}&=\frac{\partial}{\partial t}\int_{f=0}\left[\frac{A_{\alpha}S_{C}^{\alpha\beta}}{R_{\mu}M^{\mu}}\right]_{\mathrm{ret}}\mathrm{d}\mathbf{y}^{2}\\&=\int_{f=0}\left[\frac{\partial}{\partial t}\left(\frac{A_{\alpha}S_{C}^{\alpha\beta}}{R_{\mu}M^{\mu}}\right)\right]_{\mathrm{ret}}\mathrm{d}\mathbf{y}^{2}\end{aligned} \tag{A12}$$

The right side of Eq. (22) is further organized as:

$$\begin{aligned}4\pi\phi^{\beta}(\mathbf{x},t)&=\frac{\partial}{\partial X^{0}}\int_{f=0}\left[\frac{A_{\alpha}S_{C}^{\alpha\beta}}{R_{\mu}M^{\mu}}\right]_{\mathrm{ret}}\mathrm{d}\mathbf{y}^{2}\\&-\int_{f=0}\left[\frac{B_{\alpha}S_{C}^{\alpha\beta}}{R_{\mu}M^{\mu}}\right]_{\mathrm{ret}}\mathrm{d}\mathbf{y}^{2}\\&=\int_{f=0}\left[\frac{\partial}{\partial t}\left(\frac{A_{\alpha}S_{C}^{\alpha\beta}}{R_{\mu}M^{\mu}}\right)-\frac{B_{\alpha}S_{C}^{\alpha\beta}}{R_{\mu}M^{\mu}}\right]_{\mathrm{ret}}\mathrm{d}\mathbf{y}^{2}\end{aligned} \tag{A13}$$

Following the mixed function differentiation rule and organizing the integrand in the above expression, Eq. (26) can be easily proven.